Astronomy & Astrophysics manuscript no. X_ray_Abs_ver3a
March 17, 2016
©ESO 2016

arXiv:1603.05123v1 [astro-ph.HE] 16 Mar 2016

Soft X-ray absorption excess in gamma-ray burst afterglow spectra:

Absorption by turbulent ISM

M. Tanga[1,⋆], P. Schady[1], A. Gatto[2], J. Greiner[1], M. G. H. Krause[3,1,4], R. Diehl[1], S. Savaglio[1,5,6], and S. Walch[2,7]

[1] Max-Planck-Institut für Extraterrestrische Physik, PO Box 1312, Giessenbachstr. 1, 85741, Garching, Germany
[2] Max-Planck-Institut für Astrophysik, Karl-Schwarzschild-Straße 1, D-85748 Garching, Germany
[3] Universitäts-Sternwarte München, Ludwig-Maximilians-Universität, Scheinerstr. 1, 81679 München, Germany
[4] Excellence Cluster Universe, Technische Universität München, Boltzmannstrasse 2, 85748 Garching, Germany
[5] European Southern Observatory, Karl-Schwarzschild-Straße 2, 85748 Garching, Germany
[6] Physics Dept., University of Calabria, via P. Bucci, I-87036 Arcavacata di Rende, Italy
[7] Physikalisches Institut, Universität Köln, Zülpicher Strasse 77, D-50937 Köln, Germany

ABSTRACT

Two-thirds of long duration gamma-ray bursts (GRBs) show soft X-ray absorption in excess of the Milky Way. The column densities of metals inferred from UV and optical spectra differ from those derived from soft X-ray spectra, at times by an order of magnitude, with the latter being higher. The origin of the soft X-ray absorption excess observed in GRB X-ray afterglow spectra remains a heavily debated issue, which has resulted in numerous investigations on the effect of hot material both internal and external to the GRB host galaxy on our X-ray afterglow observations. Nevertheless, all models proposed so far have either only been able to account for a subset of our observations (i.e. at $z > 2$), or they have required fairly extreme conditions to be present within the absorbing material. In this paper, we investigate the absorption of the GRB afterglow by a collisionally ionised and turbulent interstellar medium (ISM). We find that a dense (3 cm^{-3}) collisionally ionised ISM could produce UV/optical and soft X-ray absorbing column densities that differ by a factor of 10, however the UV/optical and soft X-ray absorbing column densities for such sightlines and are 2-3 orders of magnitude lower in comparison to the GRB afterglow spectra. For those GRBs with a larger soft X-ray excess of up to an order of magnitude, the contribution in absorption from a turbulent ISM as considered here would ease the required conditions of additional absorbing components, such as the GRB circumburst medium and intergalactic medium.

Key words. Gamma-ray burst: general - Galaxies: irregular - Ultraviolet: ISM - X-rays: ISM

1. Introduction

Long duration gamma-ray bursts (GRBs; duration $\gtrsim$ 2s; Kouveliotou et al. 1993) are thought to originate from the collapse of rapidly rotating massive stars (25-30 $M_{\odot}$) (Woosley & Heger 2006) and this is supported by their observed association with supernovae (SNe) of type I b/c (Galama et al. 1998; Stanek et al. 2003; Hjorth et al. 2003). With luminosities of 10^{51-52} erg/s over cosmological distances from $z = 0.0085$ (Galama et al. 1998) to $z > 8.0$ (Tanvir et al. 2009; Salvaterra et al. 2009; Cucchiara et al. 2011), and emission over most of the electromagnetic spectrum, GRBs are excellent probes of the environment of their host galaxies and any intervening absorbers (Savaglio et al. 2003; Chen et al. 2005; Fynbo et al. 2006; Savaglio 2006; Prochaska et al. 2007; Piranomonte et al. 2008; Fynbo et al. 2009; Savaglio et al. 2012; Zafar et al. 2012; Japelj et al. 2015).

Since the launch of the *Swift* satellite mission in 2004 (Gehrels et al. 2004) high quality X-ray spectra (0.3 - 10 keV) of GRB afterglows are now routinely obtained with the X-Ray Telescope (XRT; Burrows et al. 2004). The rapid arc-second localisation of GRB afterglows with the XRT, which has a detection rate of > 95% (Evans et al. 2009), has enabled quick photometric and spectroscopic follow up from ground-based observatories. These follow-up observations have provided the redshift of the burst and have resulted in high signal-to-noise (S/N) observations of the absorption features originating from the circumburst medium, host galaxy interstellar medium (ISM) and intervening absorbers in UV/optical/NIR afterglow spectra. The column densities of neutral gas inferred from Lyman-α absorption in GRB afterglow spectra indicate that a high percentage of GRB hosts are damped Lyman-α systems (DLAs; $N_{HI} > 2 \times 10^{20.0}$) or sub-DLAs ($10^{19.0} < N_{HI} < 2 \times 10^{20.0}$) (Wolfe et al. 2005; Prochaska et al. 2007; Fynbo et al. 2008; Savaglio 2012; Sparre et al. 2014; Cucchiara et al. 2015). Absorption features due to singly ionised species such as Zn II, Fe II, S II, and Si II from the ISM are regularly seen in the GRB UV/optical afterglow spectra. On the basis of temporarily varying lines of singly ionised species due to photo-excitation by UV afterglow photons, the absorbing gas can be located at a distance of a few 100 pc from the GRB progenitor (e.g. Vreeswijk et al. 2007; D'Elia et al. 2011; Vreeswijk et al. 2013; Hartoog et al. 2013; Krühler et al. 2013). Absorption from highly ionised species within the host galaxy, such as C IV, N V, O VI and Si IV, are more challenging to detect because they lie within the Lyman-α forest, and they have weaker line strengths. However, their detection has been

⋆ E-mail: mohit@mpe.mpg.de

reported in a dozen GRB afterglows at $z > 2$ (Prochaska et al. 2008; Fox et al. 2008). The highly ionised species are located either within the circumburst medium of the GRB, < 20 pc from the progenitor, or within the ISM at distances of > 400 pc from the GRB progenitor, and can extend into the halo of the GRB host (Fox et al. 2008).

The soft X-ray spectra of 60% of GRBs show absorption in excess of Milky Way absorption (Evans et al. 2009; Campana et al. 2010, 2012; Starling et al. 2013). However, the nature and location of the soft X-ray absorbing material is not clear, since the narrow line absorption/emission features in soft X-ray spectra are not resolved with the *Swift*/XRT. Although ASCA (Tanaka et al. 1994), BeppoSAX (Boella et al. 1997), Chandra (Weisskopf et al. 2000) and XMM-Newton (Jansen et al. 2001) X-ray observatories are capable of resolving narrow line features, this possibility is impeded by typically long delays before the GRB observations begin by which time the X-ray afterglow has dimmed significantly. Previously claimed X-ray absorption and emission features in pre-Swift GRB afterglow spectra (Piro et al. 1999; Yoshida et al. 1999; Antonelli et al. 2000; Piro et al. 2000; Yoshida et al. 2001; Reeves et al. 2003; Butler et al. 2003; Watson et al. 2003) have been largely put in doubt (Sako et al. 2005).

The interstellar gas absorbs X-rays largely independent of temperature as long as this gas is not fully ionised. Therefore the cold neutral, warm ionised and hot ionised phases of the ISM are equally opaque to soft X-rays. The equivalent hydrogen column density (N_{HX}) inferred from absorption in soft X-ray spectra is greater than the host neutral hydrogen column density (N_{HI}) in a high percentage of GRBs (Watson et al. 2007; Campana et al. 2010) with the difference at times exceeding a factor of ten. The N_{HX} for GRBs with known redshift is measured by fitting the broad soft X-ray absorption with a neutral absorber, and then converting the best-fit metal column density to an equivalent neutral hydrogen column density assuming solar abundances. GRBs preferentially occur in subsolar metallicity environments (Le Floc'h et al. 2003; Modjaz et al. 2008; Savaglio et al. 2009; Graham & Fruchter 2013) and if this is considered, N_{HX} would increase further. The soft X-ray absorption traces the total metal content along the GRB line of sight rather than the hydrogen content and thus one should compare neutral metal column densities with the total metal column densities to estimate the excess X-ray absorption. Schady et al. (2011) compared GRB host column densities of singly and highly ionised species with the soft X-ray absorbing metal column densities rather than the neutral hydrogen column densities and concluded that these species were insufficient to account for the excess soft X-ray absorption. Instead they postulated that a significant component of ultra-highly ionised gas that is transparent to UV photons could be responsible for the excess absorption.

Other investigations into this problem have concentrated on sources of absorption that are both intrinsic and external to the GRB host galaxy. Campana et al. (2010, 2012) and more recently Starling et al. (2013), analysed a large sample of *Swift* GRBs with known redshift, and found that N_{HX} increased with redshift, implying that the soft X-ray absorption excess has an external origin. Behar et al. (2011) found that the opacity of GRBs beyond $z = 2$ remains constant, and suggested that a low redshift neutral and diffuse intergalactic medium (IGM) with metallicity of 0.2-0.4$Z_\odot$ could be the X-ray primary absorber for GRBs at high redshift ($z \gtrsim 2.0$). Similarly, Starling et al. (2013) conclude that a warm-hot IGM (WHIM) with temperatures between 10^{5-6} K and metalicity > 0.2$Z_\odot$ could explain the excess absorption for GRBs at $z \gtrsim 3$. However, recent results from surveys of intergalactic O VI absorbers at low redshift with HST show that the median metalicity (of IGM gas) at $T \sim 10^{5.5}$ K is 0.1$Z_\odot$ (Savage et al. 2014). On the basis of cosmological simulations Campana et al. (2015) show that metals in the circumgalactic medium (T $\sim$ 10^{6-7} K; 0.2 – 0.4$Z_\odot$) expelled by galactic winds from dense groups of small galaxies at low redshift can account for soft X-ray absorption in GRBs at $z \gtrsim 3$. For GRBs at $z < 2$, the contribution to the soft X-ray absorption from components external to the GRB host galaxy are expected to be $N_{HX} < 10^{22}$ cm^{-2}. On the other hand, Watson & Jakobsson (2012) have previously argued that selection effects may produce the $N_{HX} - z$ correlation, and when low redshift, dust obscured GRBs with high N_{HX} ($> 10^{22}$ cm^{-2}) are included in the GRB samples, the significance of this correlation is greatly reduced, thereby suggesting that the IGM plays a lesser role in causing excess soft X-ray absorption.

Absorption by sources internal to the GRB host have been suggested owing to the fact that N_{HX} is larger for bursts with higher N_{HI} (Krühler et al. 2011, 2012b; Campana et al. 2012; Watson et al. 2013). On the basis of both a positive correlation between N_{HX} and line of sight host dust extinction (A_V), and also between N_{HX} and N_{HI}, Watson et al. (2013) attribute the soft X-ray absorption to dense H II regions of the GRB host. Since singly ionised helium produces a soft X-ray absorption profile similar to neutral hydrogen without absorbing UV photons, Watson et al. (2013) suggest that He II in low metallicity, dense H II regions (10^{3-4} cm^{-3}) within 5 pc of the GRB is the dominant source of the absorption. Higher column densities of He would increase the X-ray opacity within the H II region by almost an order of magnitude. Krongold & Prochaska (2013) , who studied the time-dependant photoionisation of the circumburst environment by the afterglow, found that a soft X-ray excess $\gtrsim 10$ can be explained if the progenitor is embedded in a dense molecular cloud with a density that is $\sim 10 - 100$ times higher than the ISM, and is partially ionised out to 5 – 30 pc. In their simulations, solar metallicities within the dense absorbing material were required to produce an order of magnitude difference in X-ray and UV absorbing column densities. However, the largest problem that these models face is in explaining how such a highly ionised dense medium could remain in pressure equilibrium with the cold and dense neutral phase ISM.

Given the continual lack of a clear explanation for the soft X-ray absorption excess, in this paper we explore the effect of hot gas within the GRB host ISM may have on our X-ray afterglow observations. Since GRBs are associated with massive stars and SNe, the ISM of such galaxies is likely to be turbulent (e.g. Ostriker & Shetty 2011; Walch et al. 2011; de Avillez & Breitschwerdt 2012), with large volume filling factors of hot and ultra-highly ionised gas, as has been observed in a number of GRB hosts (Fox et al. 2008). We aim to understand the imprint that such an ISM would have on the GRB afterglow spectra, with a particular focus on how the ultra-highly ionised species traced by, C V, N VI and O VII affect the afterglow absorption.

To do this, we consider data cubes obtained from simulations of a multiphase and turbulent ISM driven by SNe with gas that is in collisional ionisation equilibrium (CIE). We pass random lines of sight through the data cubes and keep track of the absorbing column of all C, N, and O ions along each line of sight. The paper is organised as follows: In section 2 we discuss the expected turbulence in the ISM within GRB host galaxies, provide details of the ISM data cubes that we used, and describe our line-of-sight code used to determine the hydrogen and metal column densities. In section 3 we describe how we estimate the X-ray excess absorption from the measured column densities and com-

pare our results to observations. We discuss our results in section 4 and we provide a summary of our results in section 5.

2. Methodology

2.1. Turbulent ISM: A property of low mass star-forming galaxies

Turbulence within the ISM is driven by massive stellar feedback (e.g. Ostriker & Shetty 2011; Kim et al. 2013). GRB hosts have high SFR (e.g. Savaglio et al. 2009), are associated with SN explosions and are thus likely to have a turbulent ISM.

Host galaxies of GRBs have a typical mass of $\sim 10^9 M_\odot$ and like most low mass ($< 10^{10} M_\odot$) star-forming galaxies (SFGs) are often seen to be irregular and clumpy (Fruchter et al. 2006). These consist of star-forming clumps and lack a central bulge (e.g. Elmegreen & Elmegreen 2005; Förster Schreiber et al. 2011). The kinematics inferred from H-α line emission suggest that SFGs are rotating disks or are dominated by random motion (e.g. Förster Schreiber et al. 2006; Newman et al. 2013). The H-α emission-line studies and resolved maps of such galaxies show their ISM to be turbulent with large outflows (e.g. Newman et al. 2012). Milvang-Jensen et al. (2012) find that GRB hosts are Lyman$-\alpha$ emitters with equivalent widths larger than bright Lyman break galaxies (LBGs). Fox et al. (2008) report all seven GRBs in their sample to be absorbed by high velocity (few 100 km/s), highly ionised gas within the host galaxy, and Thöne et al. (2007) report absorption by high velocity, low ionised gas clouds possibly from the halo of the host galaxy, all of which are indicative of star formation driven outflows.

Massive star winds and SN explosions inject energy into the ISM causing it to heat up and expand. These regions of hot gas form SN bubbles extending out to kpc scales (de Avillez & Breitschwerdt 2004; Krause et al. 2013) have a low particle density and exist in dynamic equilibrium with high density and low temperature neutral gas creating a multiphase ISM. We consider simulations of an ISM that employ these properties.

2.2. Interstellar medium data cubes

Details of the three-dimensional ISM data cubes that we used are given in Gatto et al. (2015). In summary, the size of the box is 256 pc^3 with a resolution of 2 pc. The two data cubes we used for this work had an initial hydrogen density of 1 cm^{-3} and 3 cm^{-3}, and we label them as datacube1 and datacube3 for the rest of the paper. Simulations with initial temperature of 5000 K were driven artificially for 25 Myr prior to the onset of the SN explosions. Thereafter, turbulence in these boxes is driven by type II SN explosions, where the SNe are placed at random peaks at all times for datacube1, and at density peaks for 50% of the time and at random positions for the other 50% for datacube3. SN explosions at peak position correspond to SNe that explode within their natal region, while the SN explosions at random positions correspond to SN explosions from runaway stars. In the latter case, the SN explosion is more likely to occur in the ISM phase with largest volume filling factor and thus low density gas. The higher the density of the ambient medium of a SN, the more of the energy injected by the SN that is radiated away, and the lower the energy transfered to the ISM. Thus ISM with peak SN explosions causes a low fraction of hot gas within the ISM, and Gatto et al. (2015) conclude that these simulations do not produce a realistic ISM. However, they further demonstrate that as the density of the ISM data cube increases to ≥ 3 cm^{-3}, purely random SN explosions cause the ISM data cubes to be completely filled with hot gas due to a lack of radiative cooling and lack of gas outflows because of the strict periodic boundary conditions employed for the simulations. We thus restrict our analysis to the data cube with density 1 cm^{-3} with SNe placed at random positions, and the data cube with density 3 cm^{-3} with SN explosions distributed equally between peak and random positions.

The SN rates for simulations with densities 1 cm^{-3} and 3 cm^{-3} are set at 3 Myr^{-1} and 14 Myr^{-1}, respectively. The SN rate is chosen to be proportional to the star formation rate (SFR), where the latter is assumed to follow the Kennicutt-Schmidt relation (Kennicutt 1998). Using a Chabrier initial mass function (IMF) (Chabrier 2003) and star formation efficiency of 1% this corresponds to one SN per 10^2 $M_\odot$ of stellar mass formed with a predefined thermal energy of 10^{51} erg. The simulations with densities 1 cm^{-3} and 3 cm^{-3} were run for 130 Myr and 198 Myr, respectively. We use two simulations with different gas densities to see if a relation between the ISM type and X-ray absorbing gas exists. The densities of carbon, atomic hydrogen, and molecular hydrogen are given as inputs. Solar abundance ratios are assumed for both the simulations. Although GRBs are typically found to reside within subsolar metallicity galaxies (Le Floc'h et al. 2003; Modjaz et al. 2008; Savaglio et al. 2009; Graham & Fruchter 2013), for metallicities in the range $1.0Z_\odot > Z > 10^{-3}Z_\odot$, the dynamics of the simulated ISM are a weak function of metallicity (Walch et al. 2011). While supersolar GRB hosts have been reported (Levesque et al. 2010; Savaglio et al. 2012; Krühler et al. 2012a; Graham & Fruchter 2013; Elliott et al. 2013), no GRB hosts with $Z < 10^{-3}Z_\odot$ have been observed. The lowest metallicity thus far known for a GRB host galaxy is $Z \sim 0.01Z_\odot$ (GRB050730; Starling et al. 2005, GRB090926A; Rau et al. 2010. D'Elia et al. 2010), and the average host metallicity is $\sim 0.5Z_\odot$ (Prochaska et al. 2007; Savaglio 2012). We therefore expect the filling factor of warm and hot gas in our data cube to be a fair representation of the multiphase ISM within GRB host galaxies.

The formation and cooling of ions (H I, H II and C II) and molecules (H_2, CO) are calculated as the simulations using algorithms from Glover et al. (2010) and Glover & Clark (2012), and the cooling rate for highly ionised oxygen, for example O VI, is incorporated in accordance with CIE (Gnat & Ferland 2012). Thus, our treatment of the gas under the conditions of CIE is consistent with the simulations. The gas within the injection radius is heated to $10^6 - 10^7$ K when the SN explodes, and the speed of the blast expanding within the SN bubble corresponds to the speed of sound within the local region. The superbubbles then expand adiabatically and cool correspondingly. They are, however reheated time after time with subsequent explosions.

The simulations do not take the ionisation of dense regions by UV emission from massive stars into account, and only trace the collisionally ionised gas, which is only relevant above 10^4 K. Thus all gas below 10^4 K is approximated to be neutral. Under conditions of CIE, C V, N VI, and O VII form at T $> 10^5$ K and peak at T $\sim 10^{5.5}$ K (Sutherland & Dopita 1993). Large column densities of highly ionised gas can therefore only be produced in our simulations if the fraction of volume covered by these hot-diffuse regions is high. In Fig. 1 and Fig. 2 we plot the particle number density against temperature in the left panel, and the volume-weighted probability density functions (PDFs) for temperature and density, in the middle and right panels, respectively, for datacube1 and datacube3. The general widths of the temperature and density distributions is similar to that of previous studies (e.g. de Avillez & Breitschwerdt 2004) .The middle and right panels of Fig. 1 and Fig. 2 show that the hot-diffuse regions within the ISM data cubes do indeed cover a high vol-

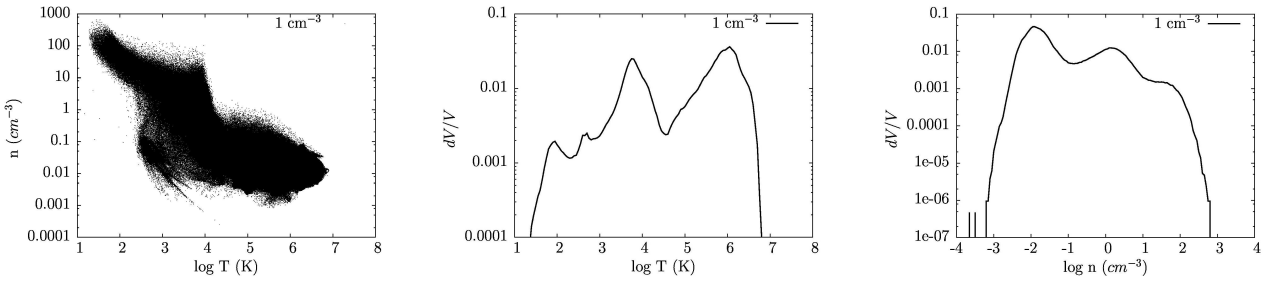

Fig. 1. ISM data cube with density 1 cm^{-3}. Left: Particle number density as a function of temperature. Middle: Volume-weighted probability density functions (PDFs) as a function of temperature. Right: Volume-weighted PDF as a function of particle number density.

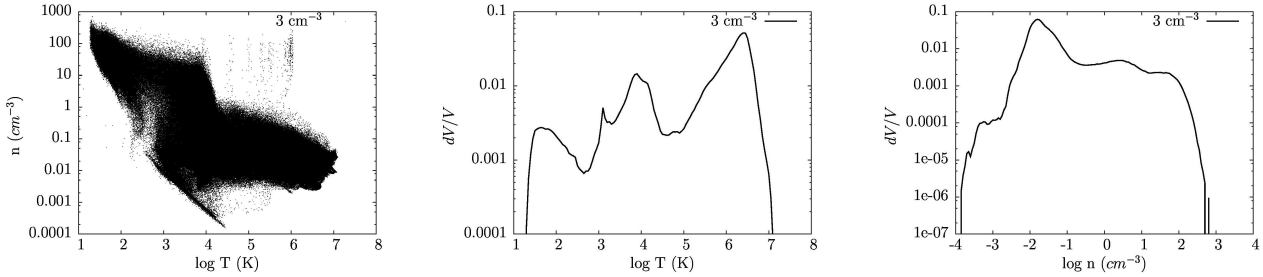

Fig. 2. As in Fig. 1 but for the ISM data cube with density 3 cm^{-3}.

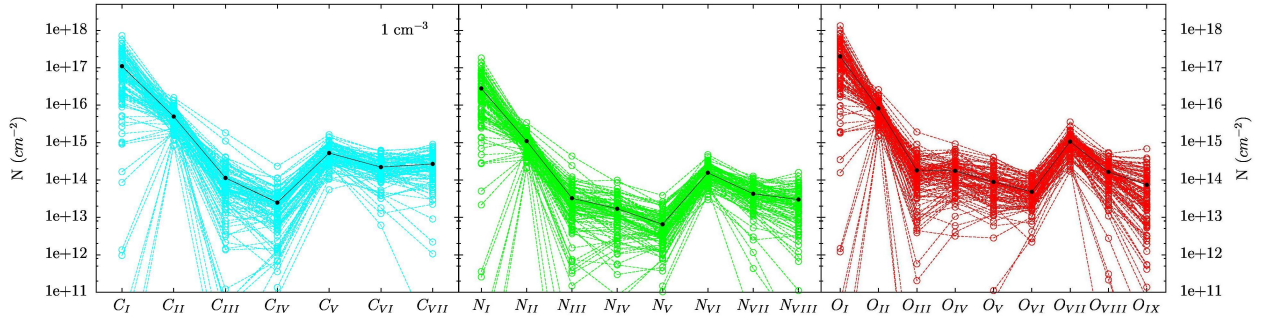

Fig. 3. Column densities of C (left), N (middle) and O (right) ions for 100 sightlines passed through our ISM data cube with density 1 cm^{-3} (datacube1). The black points indicate the average ion column densities for our 100 sightlines.

ume fraction. Fig. 2 also shows the presence of a higher volume fraction of hot and low density gas in datacube3 compared to datacube1, and a higher volume fraction of cooler gas which leads to the formation of higher densities of molecular hydrogen.

2.3. Line of sight sampling

Rays of random orientation are passed through 100 random positions within the ISM data cubes with typical path lengths ∼ 350 pc. We ensure that our sightlines sample large length scales (few 100 pc). In tracking the cells within the data cube that are crossed by our ray, only those cells where the ray crosses > 1/10 of the resolution of the cell (i.e. 0.2 pc) are considered, and we verify that no cell is selected twice. The temperature of the gas and number density of hydrogen is extracted for each selected cell, and the C, N, and O number density within each cell is calculated assuming solar abundances from Asplund et al. (2009). To calculate the ion fractions for C, N, and O, we use the CIE tables from Sutherland & Dopita (1993), which are appropriate for solar metallicities and are consistent with the assumptions that went into the data cube simulations. The distance traversed by the ray within each cell is calculated by keeping track of the entry and exit point for the cell, and the total distance traversed by the ray is then the sum of the distances traversed through all selected cells. The column densities of H, C, N, and O ions along the line of sight is the summation of their respective column densities in each cell. It is important to calculate the distance travelled within each cell to measure the column densities accurately as neither the density within the data cube nor the distances travelled within each cell are uniform.

Amongst C, N, and O, the ionisation potentials for O I and H I are most similar (13.598 eV and 13.618 eV), and thus we consider O I as a tracer of neutral gas and oxygen ion species from O I to O VIII as tracers of the X-ray absorbing gas, which we refer to as N_{OX}. The absorption excess along each sightline is estimated as the ratio of the X-ray absorbing oxygen column density, N_{OX}, to neutral oxygen column density, N_{OI}.

3. Results

Figures 3 and 4 show the distribution of C, N, and O ion column densities traced along our 100 lines of sight for datacube1

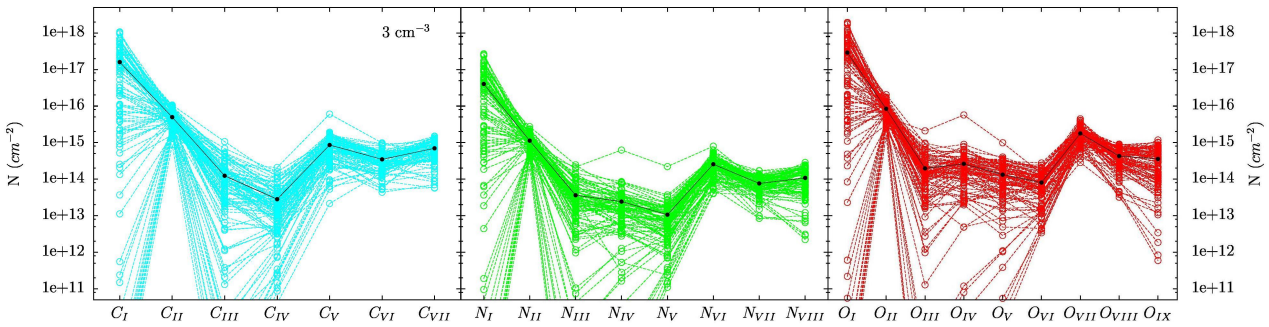

Fig. 4. As in Fig. 3 but for the ISM data cube with density 3 cm^{-3}.

Table 1. Column densities of highly ionised gas C IV, N V, O VI measured in GRB afterglow spectra (Fox et al. 2008; Prochaska et al. 2008) and along the lines of sight through our turbulent ISM data cubes(Avg., Max). Only the measured absorption from low velocity components (few 100 km/s) are given. The column densities for the ions from Fox et al. (2008) without error bars correspond to saturated lines and are uncertain.

GRB	z	N_{CIV}	N_{NV}	N_{OVI}	N_{SiIV}	Ref.
Avg. (1 cm^{-3})	...	13.40	12.82	13.68	12.65	this work
Max. (1 cm^{-3})	...	14.37	13.59	14.19	13.86	this work
Avg. (3 cm^{-3})	...	13.45	13.03	13.91	12.70	this work
Max. (3 cm^{-3})	...	14.32	14.34	14.44	13.64	this work
GRB 021004	2.32	...	14.53±0.06	14.95±0.20	15.25±0.20	1
		...	14.64±0.04	...	...	2
GRB 050730	3.97	∼ 15.24	13.80±0.14	∼ 15.94	14.16±0.06	1
		...	14.09±0.08	...	...	2
GRB 050820	2.62	13.13±0.06	13.17±0.08	...	14.91±0.07	1
		...	13.45±0.05	...	...	2
GRB 050922C	2.2	15.69±0.35	13.76±0.07	14.44±0.05	14.49±0.16	1
		...	> 14.19	...	...	2
GRB 060206	4.05	...	13.73±0.15	...	...	2
GRB 060607	3.08	15.94±0.32	...	...	13.54±0.09	1
		...	< 12.61	...	...	2
GRB 071031	2.69	∼ 15.11	14.41±0.15	∼ 15.14	15.93±0.51	1
GRB 080310	2.42	∼ 16.66	14.03±0.05	15.12±0.09	∼ 15.00	1

References. (1) Fox et al. (2008); (2) Prochaska et al. (2008).

and datacube3, respectively. For both the simulations, the column densities of ultra-highly ionised species C V, N VI and O VII are found to be similar to the neutral and singly ionised components within the H II regions (gas T > 10^4 K). However, the column densities of C I, N I, and O I increase further once the neutral ions within denser regions (gas T < 10^4 K) are considered. The column densities of C V, N VI, and O VII are generally seen to be the highest after C I, N I, O I and C II, N II, and O II, respectively. The denser data cube shows a rise in the ionisation profile at ionisation levels higher than C V, N VI, and O VII owing to the higher volume fraction of hotter ≥ 10^7 K gas in the ISM.

In Fig. 5 we plot the cumulative distribution of the soft X-ray absorption excess, $\frac{N_{OX}}{N_{OI}}$, measured along our 100 sightlines for datacube1 (green line) and datacube3 (brown line), and for comparison we also show the cumulative distribution of the excess measured in a sample of 16 GRBs (blue small-dashed line) (Schady et al. 2011; Hartoog et al. 2013; Sparre et al. 2014; D'Elia et al. 2014; Krühler et al. 2013; Friis et al. 2015). We find that 92% and 72% of the sightlines through datacube1 and datacube3, respectively, trace $\frac{N_{OX}}{N_{OI}} < 4$, and 8% and 21% of the sightlines trace $\frac{N_{OX}}{N_{OI}} > 10$. The observed $\frac{N_{OX}}{N_{OI}}$ distribution is made up of the sample of GRBs with a detected X-ray afterglow and a well-measured Zn II column density from UV/optical spectra, which are typically undepleted elements. Assuming solar relative abundances (Asplund et al. 2009), we converted the X-ray absorbing column density to an equivalent Zn column density following the method of Schady et al. (2011), and we assume that $\frac{N_{ZnX}}{N_{ZnII}} \sim \frac{N_{OX}}{N_{OI}}$. We do not consider GRBs with reported column densities from other singly ionised metals, such as Si II, S II or Fe II, due to the uncertainty in the dust depletion (e.g. Savaglio et al. 2003; De Cia et al. 2013). In Fig. 5, it can be seen that 25% of the GRBs in our sample have a soft X-ray absorption excess > 10.0 and 20% have an absorption excess < 4.0.

All GRBs within our sample have a soft X-ray absorption excess > 2.0 and thus warrant an additional absorbing component in addition to the neutral ISM. For the 25% of the GRBs with high excess > 10.0, the turbulent ISM with density 3 cm^{-3} could provide a natural explanation but the neutral and total oxygen column densities for such sightlines is 2-3 orders magnitude lower than those observed in GRB afterglow spectra (Schady et al. 2011). A high percentage of sightlines through our data cube show excess < 2.0, 86% and 63% for datacube1 and datacube3, respectively; these require an additional component to a turbulent ISM to produce the higher X-ray absorption excess. We find that the fraction of sightlines with significant absorption excess ($\frac{N_{OX}}{N_{OI}} > 2.0$) increases with density and the supernova rate,

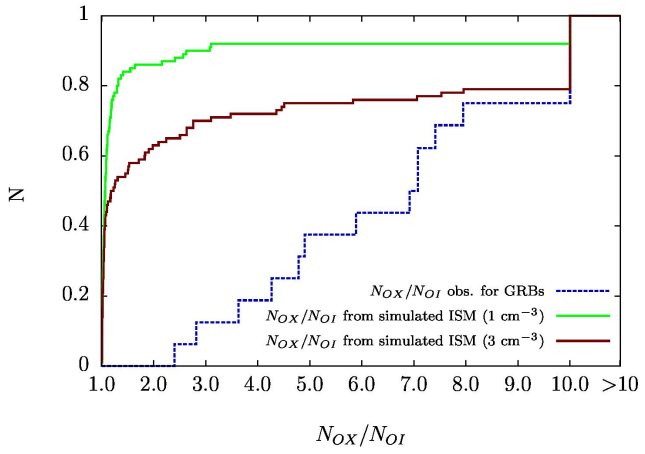

Fig. 5. Green and brown lines show the the cumulative distribution of $\frac{N_{OX}}{N_{OI}}$ for 100 sightlines crossed through our ISM data cubes with densities 1 cm^{-3} and 3 cm^{-3}, respectively, and the blue dashed line shows the observed cumulative distribution of $\frac{N_{OX}}{N_{OI}}$ for a sample of 16 GRBs.

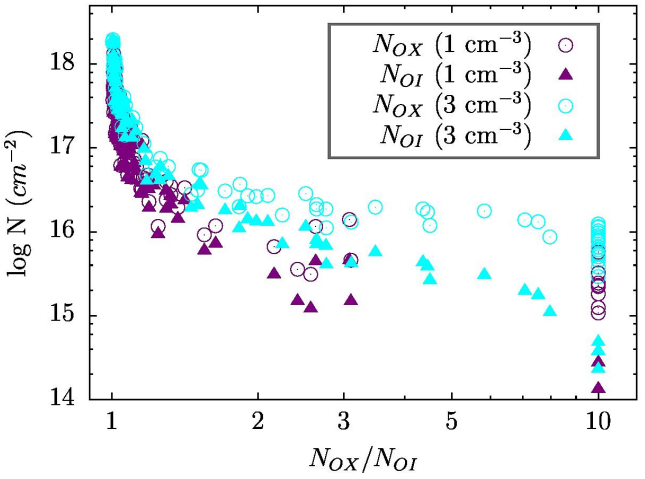

Fig. 6. N_{OX} (solid points) and N_{OI} (open points) as a function of absorption excess for 100 sightlines crossed through our ISM data cubes with densities 1 cm^{-3} (purple points) and 3 cm^{-3} (blue points).

thus a turbulent ISM with higher density than 3 cm^{-3} is a better representative of GRB host ISM.

In Fig. 6 we show N_{OX} and N_{OI} against $\frac{N_{OX}}{N_{OI}}$ for the 100 sightlines crossed through the tested ISM data cubes. We see that for both the data cubes N_{OX} remains fairly constant at $10^{15.5}$ cm^{-2} for $2 \leq \frac{N_{OX}}{N_{OI}} \leq 10$, whereas N_{OI} gradually decreases from 10^{16} cm^{-2} at $\frac{N_{OX}}{N_{OI}} = 2$, to 10^{15} cm^{-2} at $\frac{N_{OX}}{N_{OI}} = 7$ and shows a steep decline for $\frac{N_{OX}}{N_{OI}} \geq 8$. For datacube3 a high percentage $\sim 20\%$ show an absorption excess of $\frac{N_{OX}}{N_{OI}} \geq 10$, with 10^{15} cm^{-2} $\leq N_{OX} \leq 10^{16}$ cm^{-2} and $N_{OI} < 10^{15}$ cm^{-2}. This suggests that sightlines with $\frac{N_{OX}}{N_{OI}} > 2$ cross a relatively smaller volume of neutral gas rather than a higher volume of ionised gas. The contribution from cold gas to both N_{OX} and N_{OI} dominates the measured $\frac{N_{OX}}{N_{OI}}$ ratio, such that any significant X-ray excess resulting from a sightlines through a hot, diffuse cloud is rapidly diluted away by the contribution from a cold, dense cloud. This is also reflected by the increase of 2-3 orders of magnitude in both N_{OX} and N_{OI} for sightlines with $\frac{N_{OX}}{N_{OI}} < 2$.

In Table 1 we compare C IV, N V, O VI, and Si IV column densities within our data cubes with those measured within a small sample of GRB host galaxies by Prochaska et al. (2008) and Fox et al. (2008). To accomplish this, we track the Si ions in addition to the C, N, and O ions already traced. Si ions with two or more missing electrons are predominantly collisionally ionised, and thus in these cases our derived column densities are reliable. The ionisation potential of Si I is lower than H I, and thus we cannot accurately track the Si I and Si II ion fractions and column densities within the data cubes. Fox et al. (2008) reported both high velocity (few 1000 km/s) and low velocity (few 100 km/s) absorption components, and in Table 1 we report only the column densities of the low velocity absorption components, which are more likely to originate from the GRB host ISM. The velocity of the gas within the cells of our data cube is typically 10 - 100 km/s and is always below 500 km/s. We find that the measured column densities of C IV, N V, O VI, and Si IV are typically an order of magnitude larger than those traced along our 100 sightlines. For a typical GRB line of sight that crosses through a path length of 350 pc, the density of the GRB host ISM required to explain the column densities of C IV, N V, O VI, and Si IV ions should be an order of magnitude higher than the density of the ISM data cubes. Or else, the column densities can be produced by GRB host ISM with a density that is a factor of 2-3 higher than the ISM data cube and a path length of $\sim$ kpc. The later is the likely scenario given the small size of the GRB hosts ($\sim$ 5 kpc) (Fruchter et al. 2006).

We report the $\frac{N_{CIV}}{N_{OVI}}$, $\frac{N_{NV}}{N_{OVI}}$, and $\frac{N_{CIV}}{N_{SiIV}}$ ion fractions from the data cubes, and GRB afterglow spectra for the low velocity absorption components in Table 2. We also report the median of the ion ratios along with the average ratios for our 100 sightlines. The average and median ion ratios of $\frac{N_{CIV}}{N_{OVI}}$ and $\frac{N_{NV}}{N_{OVI}}$ measured along sightlines through both the ISM data cubes are comparable to the observed ratios reported in Fox et al. (2008). However, the average ion ratio of $\frac{N_{CIV}}{N_{SiIV}}$ is inconsistent with those observed in GRB afterglow spectra. Nevertheless, the median ratio of $\frac{N_{CIV}}{N_{SiIV}}$ for our sightlines through datacube1 and datacube3 are in agreement with $\frac{N_{CIV}}{N_{SiIV}}$ ion fraction observed in GRB afterglow spectra.

4. Discussion

The turbulent ISM with density 3 cm^{-3} have properties that match the observed properties such as C IV, N V, O VI, and Si IV column densities, and $\frac{N_{CIV}}{N_{OVI}}$, $\frac{N_{NV}}{N_{OVI}}$, and $\frac{N_{CIV}}{N_{SiIV}}$ ion fractions. Sightlines passed through the ISM data cube with density 3 cm^{-3} can produce the large soft X-ray absorption excess ($\frac{N_{OX}}{N_{OI}} > 10$) seen in GRB afterglow spectra. However, the total oxygen column densities for such sightlines is typically 10^{16} cm^{-2} and 2-3 orders of magnitude lower in comparison to those observed in GRB afterglow. While an ISM with higher density and larger length scale would increase N_{OX} it is unlikely that these will produce the column densities observed in GRB spectra. Also, a large fraction of sightlines do not show significant absorption excess and this is in stark contrast to the observations. In the following section we explore additional consequences such an absorbing medium has on the observations profiles that either enhance or challenge the proposed scenarios and discuss alternative sources of X-ray absorption that could be responsible for the excess X-ray absorption.

Table 2. Column density ratios for low velocity component of the highly ionised gas observed in the optical spectra of four GRBs taken from Fox et al. (2008), and the average ratios for the 100 sightlines crossed through our data cubes. The values in bracket for N_{CIV}/N_{OVI}, N_{NV}/N_{OVI}, and N_{CIV}/N_{SiIV} are the median ion ratios of our sightlines through the data cubes.

GRB	z	$\frac{N_{CIV}}{N_{OVI}}$	$\frac{N_{NV}}{N_{OVI}}$	$\frac{N_{CIV}}{N_{SiIV}}$
GRB 050730	3.97	0.40 ± 0.25	<0.09	3.7 ± 0.9
GRB 050922C	2.2	...	0.21 ± 0.04	...
GRB 071031	2.69	1.6 ± 0.4	< 0.11	3.2 ± 0.9
GRB 080310	2.42	0.55 ± 0.11	< 0.05	25 ± 4
ISM (1 cm^{-3})	–	0.63 (0.38)	0.15 (0.125)	60 (7.72)
ISM (3 cm^{-3})	–	0.55 (0.25)	0.16 (0.09)	1650 (7.75)

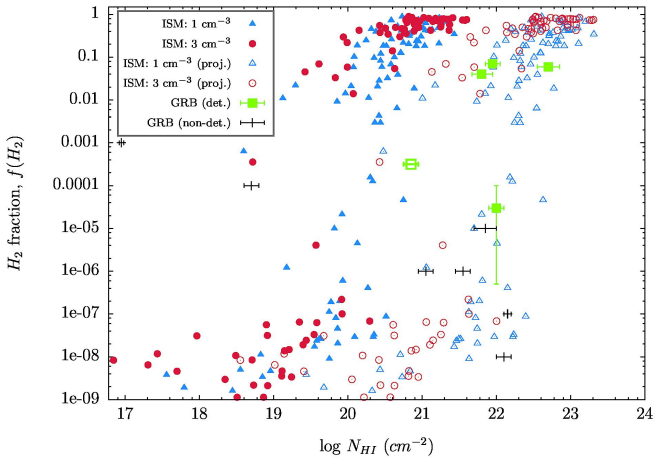

Fig. 7. Molecular hydrogen fraction ($f(H_2)$) against N_{HI} along the lines of sight for data cubes with densities 1 cm^{-3} (blue solid triangles) and 3 cm^{-3} (red solid circles). Column density of H_2, detected in GRB afterglow spectra for five GRBs (GRB 060206; (Fynbo et al. 2006), GRB 080607; Prochaska et al. (2009), GRB 120327A; D'Elia et al. (2014), GRB 120815A; Krühler et al. (2013), GRB 121014A; Friis et al. (2015)) are indicated in green and six GRBs with upper limits on $f(H_2)$ are indicated in black (Tumlinson et al. 2007; Ledoux et al. 2009). Projected N_{HI} for the $f(H_2)$ for data cubes with densities 1 cm^{-3} (blue open triangles) and 3 cm^{-3} (red open circles).

4.1. Could molecular hydrogen account for some of the excess?

Since GRB host galaxies are star-forming galaxies, and given the positive relation between molecular hydrogen and star formation (i.e. Kennicutt-Schmidt law; Kennicutt 1998; Bigiel et al. 2008), we would expect there to be an abundance of molecular gas within GRB host galaxies. We therefore consider whether molecular hydrogen could cause a notable amount of additional X-ray absorption.

Our ISM data cubes include molecular gas and thus allow us to estimate the molecular hydrogen fraction, $f(H_2) = 2N_{H_2}/[2N_{H_2} + N_{HI}]$, along the traced line of sights. In Fig. 7 we show $f(H_2)$ against N_{HI} for the 100 sightlines crossed through our ISM data cubes indicated by blue solid triangles and red solid circles for datacube1 and datacube3, respectively, for five GRBs[1] (green squares) with detected H_2 absorption in their afterglow spectra and six GRBs (black points) with upper limits on column densities of H_2 within the host ISM. As expected, for both ISM data cubes, we find that the sightlines with larger neutral metal column densities encounter a higher H_2 fraction. The observed H I column densities are larger than those measured along our sightlines through both data cubes. As noted earlier, this is due to the larger length scales probed by the GRB afterglow and/or higher density of the GRB host ISM. We scale the path of the typical path length of our sightlines to increase H I column densities for the sightlines within our data cubes to form an overlap between the detections from the GRB afterglow spectra and those are indicated with blue open triangles and red open circles for datacube1 and datacube3, respectively. For each data cube, the projected H I column densities are obtained by multiplying by a scale factor, which is given by the ratio of average N_{HI} for three GRBs with $0.01 < f(H_2) < 0.1$ to the N_{HI} within our sightlines at average $f(H_2)$ for the three GRBs. The scaled path lengths for datacube1 is ∼26 kpc and for datacube3 is ∼17 kpc, assuming typical path length of 350 pc for our sightlines.

Molecular hydrogen can absorb soft X-rays and the effective absorption excess can be estimated as $[2.85N_{H_2} + N_{HI}]/N_{HI}$, where the cross-section of H_2 is $2.85\sigma_H$ (Wilms et al. 2000). In order for H_2 to produce a soft X-ray absorption excess of > 2.0 , the H_2 fraction would then need to be > 0.5 . For all GRBs with detected H_2 absorption, the molecular hydrogen fraction is less than 0.1, and this corresponds to a soft X-ray absorption excess of less than 1.2 . Furthermore, for a sample of six GRBs with good quality optical afterglow spectra, Tumlinson et al. (2007) place an average upper limit of $10^{-6.5}$ on $f(H_2)$. On the basis of simulations, Whalen et al. (2008) show that the molecular hydrogen within the GRB vicinity would be destroyed by UV radiation from massive stars prior to the onset of GRB. They highlight the possibility, however, that absorption from molecular clouds from less active star-forming regions within the GRB host that are unrelated to the GRB progenitor region may be detected occasionally in the GRB afterglow spectra. So far, such examples of intervening molecular clouds have not been the cause for the X-ray absorption excess. For example, GRB 120327A (D'Elia et al. 2014), GRB 120815A (Krühler et al. 2013), and GRB 121014A (Friis et al. 2015) with firm detections of $f(H_2)$ and three of the GRBs in Tumlinson et al. (2007) (GRB 050820,GRB 071031, and GRB 080413) that have stringent upper limits on $f(H_2)$, are part of our sample and they have significant X-ray absorption excess ($N_{OX}/N_{OI} > 4.0$).

Although, our analysis suggests that a large H_2 fraction ($f_{H2} > 0.5$) would result in an observed X-ray excess, the excessive attenuation from gas and dust along such sightlines would typically prevent the GRB afterglows from being detected. Such sightlines could be observed in large GRB hosts with a dense ISM and with early-time sensitive spectra. These shall also lead to detection of high hydrogen fractions ($f(H_2) > 0.1$), which have been missed in observations so far (Noterdaeme et al. 2015).

[1] The detection of H_2 along the line of sight to GRB 060206 is tenuous (Prochaska et al. 2009).

Interstellar dust is unlikely to be the cause of the X-ray excess. The relation between A_V and N_{HX} along GRB lines of sight has been studied extensively. The seminal works of Galama & Wijers (2001) and Stratta et al. (2004) were the first to point out the very high gas-to-dust ratio, $\frac{N_{HX}}{A_V}$, in comparison to the Milky Way. Studies with larger samples that include heavily dust-extinguished GRBs verify this claim and have provided evidence of a positive correlation between N_{HX} and A_V (Schady et al. 2007; Starling et al. 2007; Schady et al. 2010; Greiner et al. 2011; Zafar et al. 2011, 2012; Watson et al. 2013; Covino et al. 2013). The most heavily dust extinguished GRBs are found in the most massive GRB hosts with high N_{HX} and N_{HI} (Krühler et al. 2011; Perley et al. 2013), and although N_{HX} and A_V appear to be correlated, the rate of increase in N_{HX} does not trace the increase in A_V, with $\frac{N_{HX}}{A_V}$ decreasing with an increase in A_V (Krühler et al. 2011). GRB 080607, a roughly solar metallicity GRB, is a good example, having had one of the dustiest sightlines yet detected ($A_V \sim 3.3$; Perley et al. 2011), and yet a similar N_{HX} and N_{HI}. Furthermore, most of the GRBs in the sample of Schady et al. (2011) were relatively unextinguished by dust. Thus, dust within the GRB host ISM cannot be the source of the soft X-ray absorption excess.

4.2. Additional sources of soft X-ray absorption excess in GRBs

As already stated in section 1, the alternate sources of X-ray absorption, such as as a dense circumburst medium (Krongold & Prochaska 2013), or hot IGM (Behar et al. 2011; Starling et al. 2013) face challenges. Krongold & Prochaska (2013) require the circumburst medium to be dense (> 100 cm^{-3}), pre-ionised and to extend to a few 10 pc, and how such dense hot regions of gas could exist in pressure equilibrium with the neutral phase ISM is not clear. From the density vs temperature plots for multiphase ISM, left panel in Fig. 1 and Fig. 2, we do not find gas clouds with density > 10 cm^{-3} and temperature $> 10^4$ K in a multiphase ISM. Similar conditions might however be present in young massive star clusters (e.g. Krause et al. 2012; Palouš et al. 2013) and these scenarios need to be pursued further.

Highly ionised gas, unaccounted for in our simulations, could also arise as a result of photoionisation from massive stars and delayed recombination. Photoionisation by hot stars is unsuitable to produce the high ionisation stages of oxygen (O VI and O VII),which we are primarily interested in. Soft X-ray emission (0.2 - 2 keV) from SN-remnants, superbubbles, and non-thermal sources (e.g. Sasaki et al. 2002; Haberl et al. 2012; Krause et al. 2014) scales with the star formation rate and would total to a luminosity of 10^{40} erg s^{-1} for a typical GRB host, insufficient to produce significant columns of hot gas. Non-equilibrium ionisation (NEI) may change the detailed ionisation structure compared to the collisional ionisation assumption made here (de Avillez & Breitschwerdt 2012). NEI can cause ions like C V, N VI, and O VI to be produced between $10^{3.8} \leq T \leq 10^{5.5}$ K unlike CIE conditions, where these ions can only be produced at $T > 10^5$ K. However, the soft X-ray absorption excess is measured as the ratio of total oxygen column density to the neutral oxygen column density and, thus, is insensitive to the detailed ionisation structure. We find neutral oxygen in denser regions for a collisionally ionised ISM, where collisions are frequent and delayed recombination does not have a large impact. Therefore, while the detailed NEI stage abundances would be interesting to have in this context, they would not lead to very different values for NOX and NOI. Therefore, we believe the conclusions of our analysis are robust.

Some source of hot gas, in addition to the turbulent ISM, is required to explain the observed X-ray absorption excess, and in particular, the paucity of GRBs in our sample with low soft X-ray absorption excess, $\frac{N_{OX}}{N_{OI}} < 2.0$. Absorption by collisionally ionised ISM eases the constraints on absorption by the circumburst medium and the WHIM.

5. Summary and future work

We estimate the soft X-ray absorption excess for a sample of 16 GRBs as the fraction of total oxygen column density to neutral oxygen column density, $\frac{N_{OX}}{N_{OI}}$, and we find that significant soft X-ray absorption excesses, $\frac{N_{OX}}{N_{OI}} > 2.0$, occurs in every case. Furthermore, half of the GRBs in our sample show $\frac{N_{OX}}{N_{OI}} > 10$. It is important to quantify the soft X-ray absorption for GRBs to estimate and explain the total X-ray absorbing column densities that produce this excess. In our simulations of collisionally ionised ISM, typical of star-forming galaxies such as GRB hosts, we find values of excess compatible with observations only for a small number of sightlines. In these cases, however, N_{OX} is orders of magnitude below the observed values, which are typically of the order of $10^{18.5}$ cm^{-2}. We therefore find that the ISM in GRB host galaxies cannot be the main contributor to the X-ray absorbing column for GRB afterglows. Alternate scenarios, possibly involving absorption from the circumburst medium and the WHIM, will have to be invoked to explain soft X-ray absorption excess along all the sightlines.

To obtain the observed H I column densities, the path length of the sightlines through datacube1 is required to be ∼26 kpc and the path length of the sightlines through datacube3 is required to be ∼17 kpc. GRB hosts typically are smaller in size, <10 kpc (Fruchter et al. 2006), and thus their ISM are required to be denser by a factor of 2 or 3 over 3 cm^{-3} to explain the observed H I column densities. ISM data cubes with density 10 cm^{-3} have a higher SN rate (77 Myr^{-1}) and thus a more turbulent ISM. We observe that increase in density of the ISM data cubes results in higher volume fraction of hot gas and, thus, an ISM with density 10 cm^{-3} could have a lower fraction of sightlines with $\frac{N_{OX}}{N_{OI}} < 2.0$. It seems, however, unlikely, extrapolating from the two simulations we have analysed, that the total oxygen column would increase enough to match observations.

On the basis of the ISM data cubes in our analysis, we predict the presence of ultra-highly ionised gas traced by C V, N VI, and, O VII. In Chandra and XMM-Newton X-ray observations of the Blazar outburst, K-α absorption lines from elements such as N VI and O VII produced by the WHIM have been detected, corresponding to column densities of $\sim 10^{15} - 10^{16}$ cm^{-2}, albeit with low statistical significance (e.g. Nicastro et al. 2005; Kaastra et al. 2006). The GRB afterglow soft X-ray, 0.3 – 10 keV, integrated flux at beginning of the Swift XRT observations is $\sim 10^{-10}$ erg/cm^2/s. This flux typically decays to $\sim 10^{-12}$ erg/cm^2/s after about six hours and to $\sim 10^{-13}$ erg/cm^2/s about 24 hours after the GRB trigger. The next generation of X-ray observatories such as Astro-H (Takahashi et al. 2012) and the Athena X-ray Observatory (Nandra et al. 2013) will be able to detect absorption features from ultra-highly ionised gas within the WHIM to high significance even approximately 10 hours after the GRB trigger. Such a detection with GRBs serving as beacons would be possible in ∼100 ks with Astro-H (Tashiro et al. 2014) and in ∼50 ks with X-ray IFU (Nicastro et al. 2014) on board Athena

(Barret et al. 2013). The regions of hot gas within the GRB host ISM are expected to be denser and localised within sub-kpc scales in comparison to the diffuse WHIM; the absorption signature due to the ultra-highly ionised gas within the ISM and circumburst medium should be easily detected within the exposure times required to detect the WHIM. Thus, apart from probes of the WHIM, GRBs shall serve as unique probes of the hot gas in star-forming galaxies that are ionised by massive stars.

Acknowledgements. We thank D. Breitschwerdt, D. B. Fox, and H. van Eerten for their suggestions and comments. P.S. and M.T. acknowledge support through the Sofja Kovalevskaja Award to P. Schady from the Alexander von Humboldt Foundation of Germany. This work was supported by funding from Deutsche Forschungsgemeinschaft under DFG project number PR 569/10-1 in the context of the Priority Program 1573 "Physics of the Interstellar Medium".

References

Antonelli, L. A., Piro, L., Vietri, M., et al. 2000, ApJ, 545, L39
Asplund, M., Grevesse, N., Sauval, A. J., & Scott, P. 2009, ARA&A, 47, 481
Barret, D., den Herder, J. W., Piro, L., et al. 2013, [arXiv:1308.6784B]
Behar, E., Dado, S., Dar, A., & Laor, A. 2011, ApJ, 734, 26
Bigiel, F., Leroy, A., Walter, F., et al. 2008, AJ, 136, 2846
Boella, G., Butler, R. C., Perola, G. C., et al. 1997, A&AS, 122, 299
Burrows, D. N., Hill, J. E., Nousek, J. A., et al. 2004, in Society of Photo-Optical Instrumentation Engineers (SPIE) Conference Series, Vol. 5165, X-Ray and Gamma-Ray Instrumentation for Astronomy XIII, ed. K. A. Flanagan & O. H. W. Siegmund, 201–216
Butler, N. R., Marshall, H. L., Ricker, G. R., et al. 2003, ApJ, 597, 1010
Campana, S., Salvaterra, R., Ferrara, A., & Pallottini, A. 2015, A&A, 575, A43
Campana, S., Salvaterra, R., Melandri, A., et al. 2012, MNRAS, 421, 1697
Campana, S., Thöne, C. C., de Ugarte Postigo, A., et al. 2010, MNRAS, 402, 2429
Chabrier, G. 2003, PASP, 115, 763
Chen, H.-W., Prochaska, J. X., Bloom, J. S., & Thompson, I. B. 2005, ApJ, 634, L25
Covino, S., Melandri, A., Salvaterra, R., et al. 2013, MNRAS, 432, 1231
Cucchiara, A., Fumagalli, M., Rafelski, M., et al. 2015, ApJ, 804, 51
Cucchiara, A., Levan, A. J., Fox, D. B., et al. 2011, ApJ, 736, 7
de Avillez, M. A. & Breitschwerdt, D. 2004, A&A, 425, 899
de Avillez, M. A. & Breitschwerdt, D. 2012, ApJ, 756, L3
De Cia, A., Ledoux, C., Savaglio, S., Schady, P., & Vreeswijk, P. M. 2013, A&A, 560, A88
D'Elia, V., Campana, S., Covino, S., et al. 2011, MNRAS, 418, 680
D'Elia, V., Fynbo, J. P. U., Goldoni, P., et al. 2014, A&A, 564, A38
Elliott, J., Krühler, T., Greiner, J., et al. 2013, A&A, 556, A23
Elmegreen, B. G. & Elmegreen, D. M. 2005, ApJ, 627, 632
Evans, P. A., Beardmore, A. P., Page, K. L., et al. 2009, MNRAS, 397, 1177
Förster Schreiber, N. M., Genzel, R., Lehnert, M. D., et al. 2006, ApJ, 645, 1062
Förster Schreiber, N. M., Shapley, A. E., Genzel, R., et al. 2011, ApJ, 739, 45
Fox, A. J., Ledoux, C., Vreeswijk, P. M., Smette, A., & Jaunsen, A. O. 2008, A&A, 491, 189
Friis, M., De Cia, A., Krühler, T., et al. 2015, MNRAS, 451, 167
Fruchter, A. S., Levan, A. J., Strolger, L., et al. 2006, Nature, 441, 463
Fynbo, J. P. U., Jakobsson, P., Prochaska, J. X., et al. 2009, ApJS, 185, 526
Fynbo, J. P. U., Prochaska, J. X., Sommer-Larsen, J., Dessauges-Zavadsky, M., & Møller, P. 2008, ApJ, 683, 321
Fynbo, J. P. U., Starling, R. L. C., Ledoux, C., et al. 2006, A&A, 451, L47
Galama, T. J., Vreeswijk, P. M., van Paradijs, J., et al. 1998, Nature, 395, 670
Galama, T. J. & Wijers, R. A. M. J. 2001, ApJ, 549, L209
Gatto, A., Walch, S., Low, M.-M. M., et al. 2015, MNRAS, 449, 1057
Gehrels, N., Chincarini, G., Giommi, P., et al. 2004, ApJ, 611, 1005
Glover, S. C. O. & Clark, P. C. 2012, MNRAS, 421, 116
Glover, S. C. O., Federrath, C., Mac Low, M.-M., & Klessen, R. S. 2010, MNRAS, 404, 2
Gnat, O. & Ferland, G. J. 2012, ApJS, 199, 20
Graham, J. F. & Fruchter, A. S. 2013, ApJ, 774, 119
Greiner, J., Krühler, T., Klose, S., et al. 2011, A&A, 526, A30
Haberl, F., Sturm, R., Ballet, J., et al. 2012, A&A, 545, A128
Hartoog, O. E., Wiersema, K., Vreeswijk, P. M., et al. 2013, MNRAS, 430, 2739
Hjorth, J., Sollerman, J., Møller, P., et al. 2003, Nature, 423, 847
Jansen, F., Lumb, D., Altieri, B., et al. 2001, A&A, 365, L1
Japelj, J., Covino, S., Gomboc, A., et al. 2015, A&A, 579, A74
Kaastra, J. S., Werner, N., Herder, J. W. A. d., et al. 2006, ApJ, 652, 189
Kennicutt, Jr., R. C. 1998, ApJ, 498, 541
Kim, C.-G., Ostriker, E. C., & Kim, W.-T. 2013, ApJ, 776, 1
Kouveliotou, C., Meegan, C. A., Fishman, G. J., et al. 1993, ApJ, 413, L101
Krause, M., Charbonnel, C., Decressin, T., et al. 2012, A&A, 546, L5
Krause, M., Diehl, R., Böhringer, H., Freyberg, M., & Lubos, D. 2014, A&A, 566, A94
Krause, M., Fierlinger, K., Diehl, R., et al. 2013, A&A, 550, A49
Krongold, Y. & Prochaska, J. X. 2013, ApJ, 774, 115
Krühler, T., Fynbo, J. P. U., Geier, S., et al. 2012a, A&A, 546, A8
Krühler, T., Greiner, J., Schady, P., et al. 2011, A&A, 534, A108
Krühler, T., Ledoux, C., Fynbo, J. P. U., et al. 2013, A&A, 557, A18
Krühler, T., Malesani, D., Milvang-Jensen, B., et al. 2012b, ApJ, 758, 46
Le Floc'h, E., Duc, P.-A., Mirabel, I. F., et al. 2003, A&A, 400, 499
Ledoux, C., Vreeswijk, P. M., Smette, A., et al. 2009, A&A, 506, 661
Levesque, E. M., Kewley, L. J., Graham, J. F., & Fruchter, A. S. 2010, ApJ, 712, L26
Milvang-Jensen, B., Fynbo, J. P. U., Malesani, D., et al. 2012, ApJ, 756, 25
Modjaz, M., Kewley, L., Kirshner, R. P., et al. 2008, AJ, 135, 1136
Nandra, K., Barret, D., Barcons, X., et al. 2013, [arXiv:1306.2307]
Newman, S. F., Genzel, R., Förster Schreiber, N. M., et al. 2013, ApJ, 767, 104
Newman, S. F., Genzel, R., Förster-Schreiber, N. M., et al. 2012, ApJ, 761, 43
Nicastro, F., Kaastra, J., & Finoguenov, A. 2014, in COSPAR Meeting, Vol. 40, 40th COSPAR Scientific Assembly. Held 2-10 August 2014, in Moscow, Russia, Abstract E1.9-6-14., 2271
Nicastro, F., Mathur, S., Elvis, M., et al. 2005, ApJ, 629, 700
Noterdaeme, P., Petitjean, P., & Srianand, R. 2015, A&A, 578, L5
Ostriker, E. C. & Shetty, R. 2011, ApJ, 731, 41
Palouš, J., Wünsch, R., Martínez-González, S., et al. 2013, ApJ, 772, 128
Perley, D. A., Levan, A. J., Tanvir, N. R., et al. 2013, ApJ, 778, 128
Perley, D. A., Morgan, A. N., Updike, A., et al. 2011, AJ, 141, 36
Piranomonte, S., Ward, P. A., Fiore, F., et al. 2008, A&A, 492, 775
Piro, L., Costa, E., Feroci, M., et al. 1999, ApJ, 514, L73
Piro, L., Garmire, G., Garcia, M., et al. 2000, Science, 290, 955
Prochaska, J. X., Chen, H.-W., Dessauges-Zavadsky, M., & Bloom, J. S. 2007, ApJ, 666, 267
Prochaska, J. X., Dessauges-Zavadsky, M., Ramirez-Ruiz, E., & Chen, H.-W. 2008, ApJ, 685, 344
Prochaska, J. X., Sheffer, Y., Perley, D. A., et al. 2009, ApJ, 691, L27
Reeves, J. N., Watson, D., Osborne, J. P., Pounds, K. A., & O'Brien, P. T. 2003, A&A, 403, 463
Sako, M., Harrison, F. A., & Rutledge, R. E. 2005, ApJ, 623, 973
Salvaterra, R., Della Valle, M., Campana, S., et al. 2009, Nature, 461, 1258
Sasaki, M., Haberl, F., & Pietsch, W. 2002, A&A, 392, 103
Savage, B. D., Kim, T.-S., Wakker, B. P., et al. 2014, ApJS, 212, 8
Savaglio, S. 2006, New Journal of Physics, 8, 195
Savaglio, S. 2012, Astronomische Nachrichten, 333, 480
Savaglio, S., Fall, S. M., & Fiore, F. 2003, ApJ, 585, 638
Savaglio, S., Glazebrook, K., & Le Borgne, D. 2009, ApJ, 691, 182
Savaglio, S., Rau, A., Greiner, J., et al. 2012, MNRAS, 420, 627
Schady, P., Mason, K. O., Page, M. J., et al. 2007, MNRAS, 377, 273
Schady, P., Page, M. J., Oates, S. R., et al. 2010, MNRAS, 401, 2773
Schady, P., Savaglio, S., Krühler, T., Greiner, J., & Rau, A. 2011, A&A, 525, A113
Sparre, M., Hartoog, O. E., Krühler, T., et al. 2014, ApJ, 785, 150
Stanek, K. Z., Matheson, T., Garnavich, P. M., et al. 2003, ApJ, 591, L17
Starling, R. L. C., Wijers, R. A. M. J., Wiersema, K., et al. 2007, ApJ, 661, 787
Starling, R. L. C., Willingale, R., Tanvir, N. R., et al. 2013, MNRAS, 431, 3159
Stratta, G., Fiore, F., Antonelli, L. A., Piro, L., & De Pasquale, M. 2004, ApJ, 608, 846
Sutherland, R. S. & Dopita, M. A. 1993, ApJS, 88, 253
Takahashi, T., Mitsuda, K., Kelley, R., et al. 2012, in Society of Photo-Optical Instrumentation Engineers (SPIE) Conference Series, Vol. 8443, Society of Photo-Optical Instrumentation Engineers (SPIE) Conference Series, 1
Tanaka, Y., Inoue, H., & Holt, S. S. 1994, PASJ, 46, L37
Tanvir, N. R., Fox, D. B., Levan, A. J., et al. 2009, Nature, 461, 1254
Tashiro, M. S., Yonetoku, D., Ohno, M., et al. 2014, [arXiv:1412.1179]
Thöne, C. C., Greiner, J., Savaglio, S., & Jehin, E. 2007, ApJ, 671, 628
Tumlinson, J., Prochaska, J. X., Chen, H.-W., Dessauges-Zavadsky, M., & Bloom, J. S. 2007, ApJ, 668, 667
Vreeswijk, P. M., Ledoux, C., Raassen, A. J. J., et al. 2013, A&A, 549, A22
Vreeswijk, P. M., Ledoux, C., Smette, A., et al. 2007, A&A, 468, 83
Walch, S., Wünsch, R., Burkert, A., Glover, S., & Whitworth, A. 2011, ApJ, 733, 47
Watson, D., Hjorth, J., Fynbo, J. P. U., et al. 2007, ApJ, 660, L101
Watson, D. & Jakobsson, P. 2012, ApJ, 754, 89
Watson, D., Reeves, J. N., Hjorth, J., Jakobsson, P., & Pedersen, K. 2003, ApJ, 595, L29
Watson, D., Zafar, T., Andersen, A. C., et al. 2013, ApJ, 768, 23
Weisskopf, M. C., Tananbaum, H. D., Van Speybroeck, L. P., & O'Dell, S. L. 2000, in Society of Photo-Optical Instrumentation Engineers (SPIE) Conference Series, Vol. 4012, X-Ray Optics, Instruments, and Missions III, ed. J. E. Truemper & B. Aschenbach, 2–16
Whalen, D., Prochaska, J. X., Heger, A., & Tumlinson, J. 2008, ApJ, 682, 1114
Wilms, J., Allen, A., & McCray, R. 2000, ApJ, 542, 914
Wolfe, A. M., Gawiser, E., & Prochaska, J. X. 2005, ARA&A, 43, 861
Woosley, S. E. & Heger, A. 2006, ApJ, 637, 914
Yoshida, A., Namiki, M., Otani, C., et al. 1999, A&AS, 138, 433
Yoshida, A., Namiki, M., Yonetoku, D., et al. 2001, ApJ, 557, L27
Zafar, T., Watson, D., Elíasdóttir, Á., et al. 2012, ApJ, 753, 82
Zafar, T., Watson, D., Fynbo, J. P. U., et al. 2011, A&A, 532, A143